Article

Current Biology

Acto-myosin network geometry defines centrosome position

Graphical Abstract

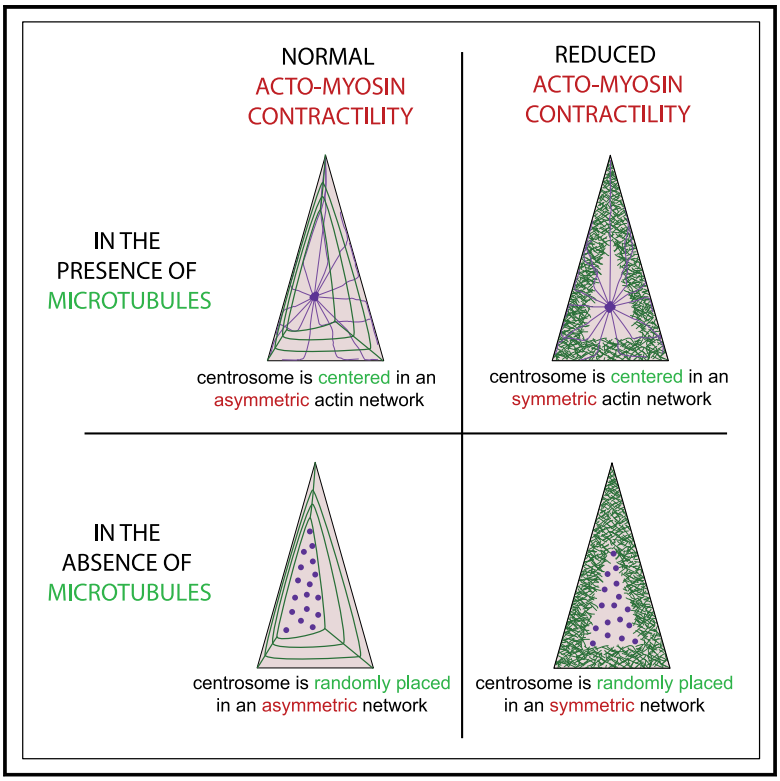

Highlights

- The centrosome-microtubule array has a nucleus-independent self-centering capacity
- Microtubules do not position the centrosome at the geometric center of the cell
- The centrosome sits at the center of a region defined by the acto-myosin network
- Dyneins are enriched in this inner region devoid of acto-myosin bundles

Authors

Ana Joaquina Jimenez, Alexandre Schaeffer, Chiara De Pascalis, ..., Matthieu Piel, Laurent Blanchoin, Manuel Théry

Correspondence

manuel.thery@cea.fr

In Brief

Jimenez et al. show that the centrosome, which has long been thought to sit at the geometric center of the cell, is actually positioned at the center of a subcellular zone defined by the absence of contractile acto-myosin bundles. Centrosome position is defined by dyneins exerting pulling forces on microtubules specifically in this zone.

Jimenez et al., 2021, Current Biology *31*, 1–15
March 22, 2021
https://doi.org/10.1016/j.cub.2021.01.002

CellPress

Please cite this article in press as: Jimenez et al., Acto-myosin network geometry defines centrosome position, Current Biology (2021), https://doi.org/10.1016/j.cub.2021.01.002

Current Biology

CellPress

Article

Acto-myosin network geometry defines centrosome position

Ana Joaquina Jimenez,[1] Alexandre Schaeffer,[1] Chiara De Pascalis,[1] Gaëlle Letort,[2] Benoit Vianay,[1] Michel Bornens,[3] Matthieu Piel,[3,4] Laurent Blanchoin,[1,5] and Manuel Théry[1,5,6,7,*]

[1]University of Paris, CEA, INSERM, Institut de Recherche Saint Louis, UMRS1160-HIPI, CytoMorpho Lab, Avenue Claude Vellefaux, 75010 Paris, France

[2]CIRB, Collège de France, UMR7241/U1050, Place Marcelin Berthelot, 75005 Paris, France

[3]Institut Curie, PSL Research University, CNRS, UMR 144, Paris, France

[4]Institut Pierre Gilles de Gennes, PSL Research University, Paris, France

[5]University of Grenoble-Alpes, CEA, CNRS, INRA, Interdisciplinary Research Institute of Grenoble, UMR5168-LPCV, CytoMorpho Lab, Avenue des Martyrs, 38054 Grenoble, France

[6]Twitter: @manuelthery

[7]Lead contact

*Correspondence: manuel.thery@cea.fr

https://doi.org/10.1016/j.cub.2021.01.002

SUMMARY

The centrosome is the main organizer of microtubules and as such, its position is a key determinant of polarized cell functions. As the name says, the default position of the centrosome is considered to be the cell geometrical center. However, the mechanism regulating centrosome positioning is still unclear and often confused with the mechanism regulating the position of the nucleus to which it is linked. Here, we used enucleated cells plated on adhesive micropatterns to impose regular and precise geometrical conditions to centrosome-microtubule networks. Although frequently observed there, the equilibrium position of the centrosome is not systematically at the cell geometrical center and can be close to cell edge. Centrosome positioning appears to respond accurately to the architecture and anisotropy of the actin network, which constitutes, rather than cell shape, the actual spatial boundary conditions the microtubule network is sensitive to. We found that the contraction of the actin network defines a peripheral margin in which microtubules appear bent by compressive forces. The progressive disassembly of the actin network at distance from the cell edges defines an inner zone where actin bundles were absent, where microtubules were more radially organized and where dynein concentration was higher. We further showed that the production of dynein-based forces on microtubules places the centrosome at the center of this zone. In conclusion, the spatial distribution of cell adhesion and the production of contractile forces define the architecture of the actin network with respect to which the centrosome-microtubule network is centered.

INTRODUCTION

The centrosome position is intimately associated to polarized cell functions such as adsorption and secretion, motility, and mitosis.[1] Its position is characteristic and indicative of polarized cell functions.[2] It is found at the cell center in proliferating cells in culture, whereas it presents a peripheral position in differentiated cells in tissues, where it loses part or all of its functions in microtubule organization.[3–5] During several cellular events essential to development, and organism homeostasis, the centrosome position undergoes a shift from the center to periphery of the cell, notably during ciliogenesis,[6] neuronal developement,[7] immune synapse formation,[8] or epithelial-to-mesenchymal transition.[9] However, the mechanisms that regulate the stability of central and peripheral states and those that allow a rapid switch between two states have not yet been fully understood.

Previous *in vivo*, *in vitro*, and *in silico* studies suggest that centrosome position is the outcome of a balance of pulling and pushing forces applied on microtubules and transmitted to the centrosome.[10,11] Overexpression or depletion of dynein heavy chains or its partners, and injections of dynein blocking antibodies suggest cortical and cytoplasmic dynein play a role in the production of pulling forces for the centrosome position.[12–16] Besides, microtubule polymerization against spatial boundaries have been shown to be responsible for the production of pushing forces.[17–19] The exact role of actomyosin contraction is unclear. The inhibition of actomyosin contraction had no visible effect on centrosome position in isolated cells or in monolayers;[20] however, it was found capable of counteracting the centrosome shift due to local microtubule disassembly[12] and of perturbing centrosome repositioning at the cell center after mitosis.[21]

In non-differentiated cells, and notably in cells proliferating in culture, the force balance is believed to set the centrosome position at the cell geometrical center, also called center of mass or centroid.[4,20,22,23] Microtubule-based forces in an *in vitro* reconstituted system also position the microtubule-organizing center

Please cite this article in press as: Jimenez et al., Acto-myosin network geometry defines centrosome position, Current Biology (2021), https://doi.org/10.1016/j.cub.2021.01.002

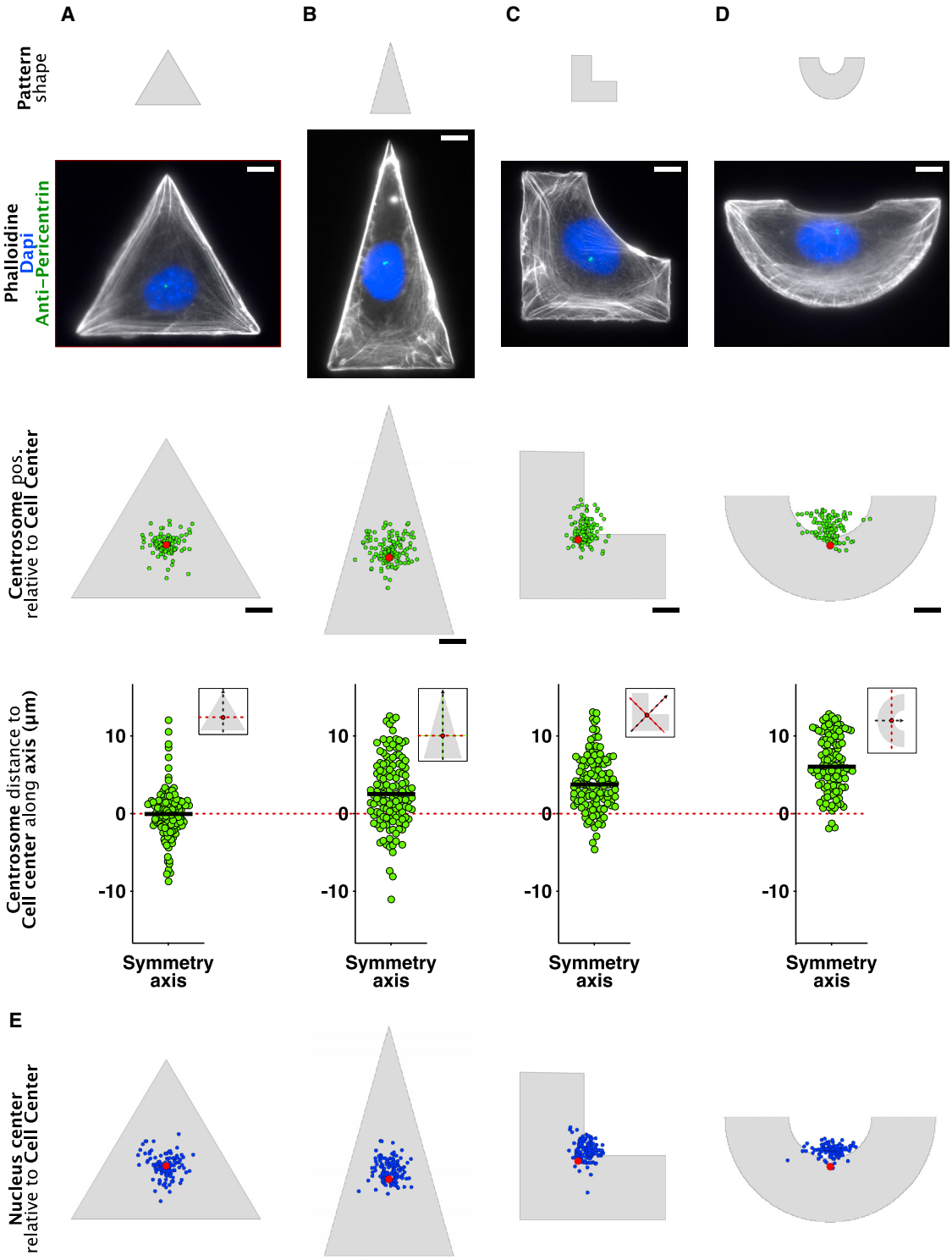

Figure 1. Centrosome is shifted from the geometrical center in cells plated on anisotropic adhesion micropatterns

(A–D) MEF WT cells were seeded on 2,000 μm^2 equilateral triangles (n = 128) (A), isosceles "short" triangles (n = 131) (B), L shapes (n = 125) (C), or U shapes (n = 121) (D). Cells were stained for actin by using Phalloidine-A555 and with anti-Pericentrin to label the centrosome. Graphs show centrosome distribution in relation to cell centroid. Plots correspond to the centrosome distance to cell centroid along the axis indicated by dashed black arrows. Dashed red line is perpendicular to black axis and passes by cell centroid.

(E) Nucleus centroid distributions in relation to cell centroid, as indicated. Similar experiments are shown in Figures S1A and S1B, for RPE1 and C2C12 cells. Scale bar, 10 µm.

Please cite this article in press as: Jimenez et al., Acto-myosin network geometry defines centrosome position, Current Biology (2021), https://doi.org/10.1016/j.cub.2021.01.002

CellPress

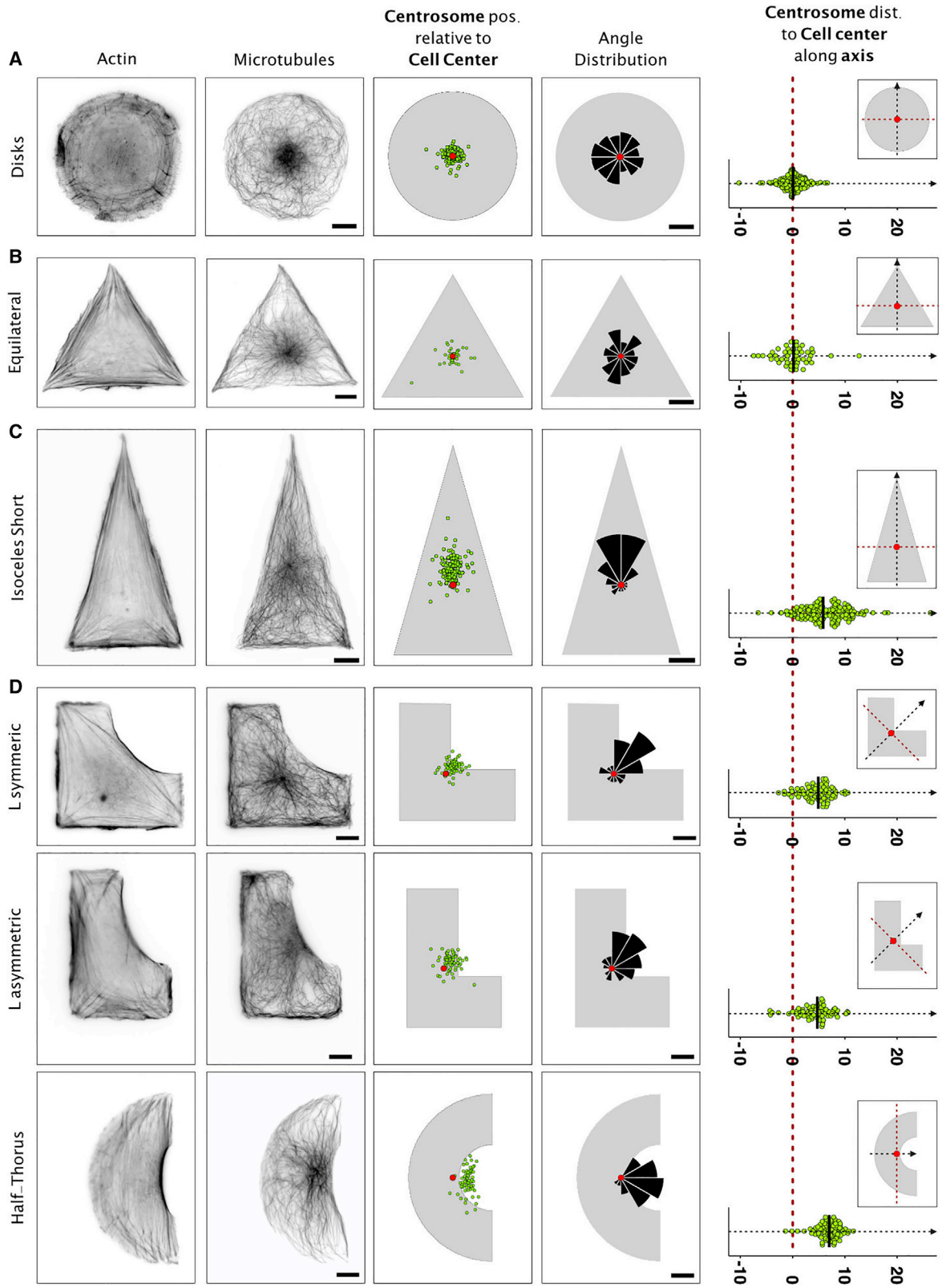

Figure 2. Centrosome positioning at and away from the cell geometrical center in enucleated cells

(A–D) Cytoplasts from MEF KO vimentin cells expressing EGFP-Centrin1 were made, as illustrated in Figure S1C. They were plated on micropatterns of different shapes with a constant area of 2,000 μm^2: discs (n = 147) (A), equilateral triangle (n = 47) (B), isosceles triangle 7:4 ratio (n = 147) (C), and anisotropic micropatterns

(legend continued on next page)

Please cite this article in press as: Jimenez et al., Acto-myosin network geometry defines centrosome position, Current Biology (2021), https://doi.org/10.1016/j.cub.2021.01.002

(MTOC) at the centroid of their confinement area,[24] but *in silico* simulation suggested this mechanism might depend on the shape and physical properties of the boundaries.[25,26] Indeed, in cultured cells, the centrosome has been observed at the cell geometrical center in relatively isotropic boundary conditions (e.g., non-polarized cells) but can be off-centered in the front or in the back of migrating cells[27–29] or toward the intercellular junction in epithelial cells.[9,30] As a result, there is no generic definition of the centrosome position, and the key parameters involved in the regulation of this positioning are still unclear.

One limitation for the identification of the forces exerted on the centrosome is that the mechanism of centrosome positioning is hardly distinguishable from nucleus positioning. It has been a considerable limitation for the study of centrosome positioning in anisotropic conditions such as in migrating cells.[31,32] Both the nucleus and the centrosome have their own self-centering properties.[10,33,34] However, the physical links that connect them hinder their respective contributions in regard to their final position.[35–39] In addition, the nucleus also constitutes a dead volume microtubules don't have access to, which biases the spatial distribution of microtubules and their associated forces.[28] Furthermore, centrosomal microtubules push and pull on the nuclear envelope,[40–42] adding more complexity to the force balance in the centrosome-microtubule network. For these reasons, enucleated cells —here referred to as cytoplasts—offered an interesting possibility to untangle the geometrical and molecular cues that specifically control centrosome position.[43] Plating them on adhesive micropatterns revealed that centrosome self-positions at the geometrical center of the cytoplasts suggesting that its off-centering in cells is due to microtubule interaction with the nucleus.[23,32] However, the centrosome often detaches from the nucleus when moving to the cell periphery during the migration of neuroblasts[44] or epithelium formation,[45] for example. This might indicate that the centrosome-microtubule network could be powered by active off-centering properties independently of the nucleus, although this has not yet been demonstrated.

Here, we show that actin contractile network plays an important role in the confinement of the microtubule networks whereas the positioning of the centrosome at the center of this actin-based boundary is achieved by dynein-based forces on microtubules.

RESULTS

Centrosome is off-centered in cells plated on anisotropic adhesion pattern

The centrosome of mouse embryonic fibroblasts (MEFs) was located at the geometrical center of cells plated on relatively isotropic adhesive patterns such as equilateral triangles (Figure 1A), as previously described.[20] However, it appeared shifted from the geometrical center when cells were plated on isosceles triangle, despite the fact that in these conditions cells were not migrating or forming contact with any adjacent cells (Figure 1B). With that micropattern, the actin-network architecture was polarized, and not just a homothetic transformation of the cell contour. The width of the network was greater along the triangle's base, and the arrangement of actin bundles differed between the larger vertices and the smaller apex (Figure 1B). This suggested that the centrosome positioning away from the geometric center could be due to the asymmetry in the actin network. To further investigate this possibility, actin-network asymmetry was reinforced. Previous work has shown that the distribution of the cell's adhesions to a substrate can direct the architecture of the actin network,[46–48] and this can be achieved by plating a cell on a micropattern such that the cell adopts a convex edge and a concave edge. In this situation, the actin network tends to flow from sites of cell-substrate adhesions at the convex edge, toward sites between cell substrate adhesion at the concave edge where stress fibers tend to form. Thus, cells were plated on L-shaped or C-shaped micropatterns to impose asymmetric actin network architecture. With both micropatterns, the actin network displayed a marked asymmetry, and the centrosome was significantly shifted from the geometric center, in the direction of the actin-network retrograde flow toward the edge harboring contractile stress fibers (Figures 1C and 1D). Similar shift was observed in human retinal pigment epithelial (RPE1) cells and mouse muscle myoblast (C2C12) (Figures S1A and S1B). This supported the idea that centrosome positioning is affected by the pattern of cell adhesions and the architecture of the actin network.

However, the nucleus position was also shifted from the cell geometrical center when cells were plated on anisotropic micropatterns (Figure 1E). So it was unclear whether the centrosome was off-centered because it was attached to an off-centered nucleus or whether the microtubule-centrosome network was not self-centering with respect to cell shape in those conditions.

Centrosome is off-centered in cytoplasts plated on anisotropic adhesion pattern

Cell enucleation allows the study of centrosome-microtubule network interaction with cell peripheral boundary without the bias of the interaction with the nucleus. Cytoplasts, i.e., enucleated cells, were produced by centrifugation of attached cells on extracellular matrix (ECM)-coated plastic slides.[49] They were then detached and plated on large 2,000 μm^2 disc-shaped micropatterns, in order to maximize their spreading and the available space for centrosome positioning in 2D. However, we found that the major network of vimentin intermediate filament in fibroblasts and RPE1 cells forms a dense network around the nucleus,[50] which can resist enucleation, maintain its perinuclear architecture, and affect microtubule network organization (Figure S1D). To avoid any geometrical bias due to intermediate filaments, we further worked with vimentin-KO MEFs when possible (and if not specified otherwise).[50–52] In these cells, centrosomes were found to precisely position at the cell geometrical center of isotropical shapes: 84% were found in a 5 μm wide region at the center of the disc (Figure 2A) or of equilateral triangles (Figure 2B). On discs, centrosomes displayed similar centering

(D), symmetric L (n = 73), asymmetric L (n = 70), and U shapes (n = 76). For each shape, an example of actin and microtubule networks is presented. More exotic shapes are presented in Figure S3A and examples in C2C12 cells are shown in Figure S3B. The plots represent, from left to right, the distribution in relation to the cell centroid of centrosome position, the angle distribution and centrosome distance along the axis indicated by dashed-black arrows. Dashed red line is perpendicular to black axis and passes by cell centroid. For further geometrical analysis of triangle shapes see Figure S2. Scale bars, 10μm.

Please cite this article in press as: Jimenez et al., Acto-myosin network geometry defines centrosome position, Current Biology (2021), https://doi.org/10.1016/j.cub.2021.01.002

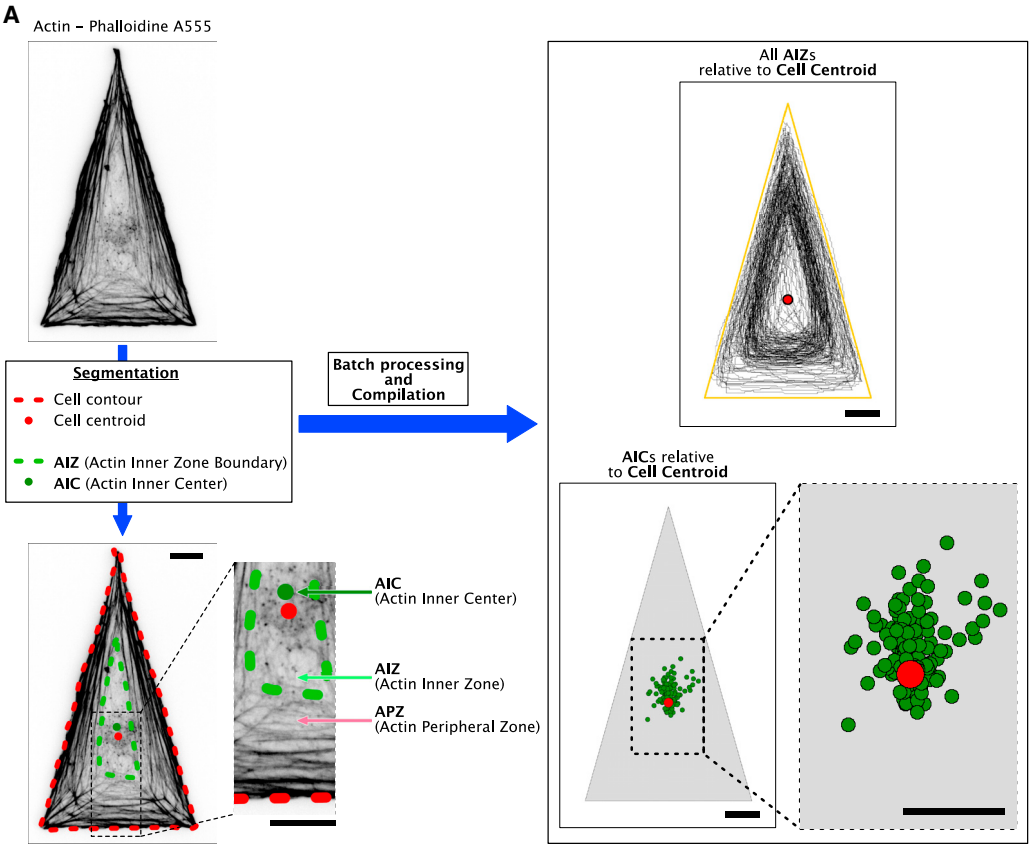

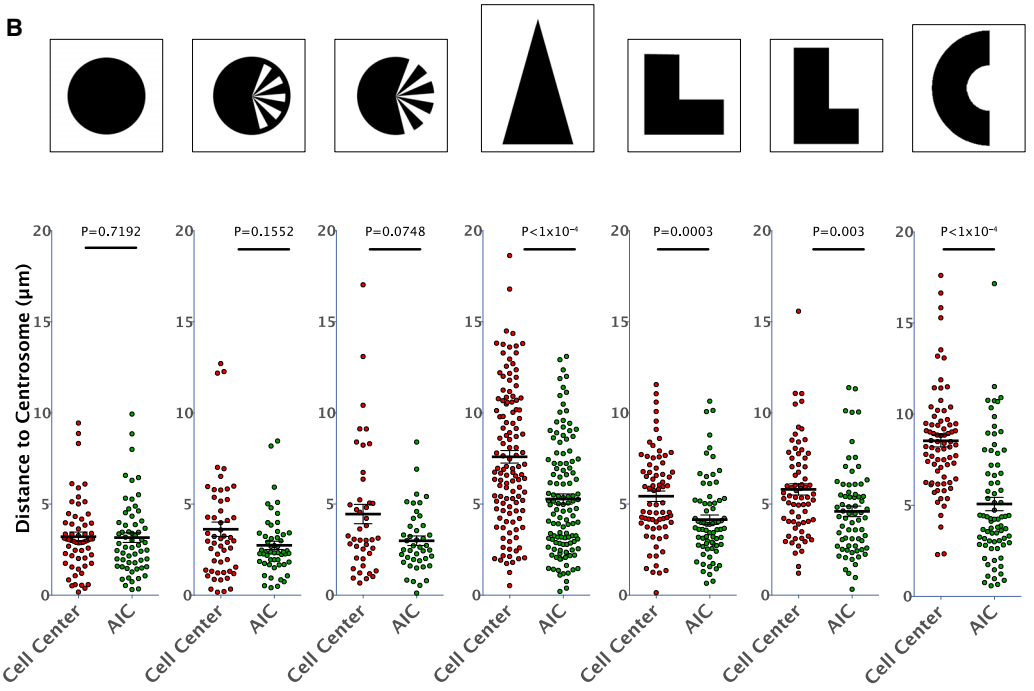

(legend on next page)

Please cite this article in press as: Jimenez et al., Acto-myosin network geometry defines centrosome position, Current Biology (2021), https://doi.org/10.1016/j.cub.2021.01.002

efficiency in cells and the cytoplast, with or without the vimentin network (Figure S1E).

In order to investigate centrosome positioning in anisotropic conditions, we plated cytoplasts expressing enhanced green fluorescent protein (EGFP)-Centrin1 on a variety of triangular geometries. We first chose triangles of similar area but different height-to-bases ratio: equilateral, short isosceles (ratio 7:4) and isosceles (ratio 9:2) (Figures 2B, 2C, and S2). Thousands of different geometrical centers have been described in triangles.[53] We measured centrosome position in relation to some centers that are interesting because their definition presumes simple relationship with the sides or the vertexes of the triangle. Those are the circumcenter (equidistant to the triangle vertexes), the incenter (equidistant to the triangle sides), the geometrical center (which reflects the entire area of the triangle), and the orthocenter—which minimizes the sum of its distances to the triangle vertexes and to those of its pedal triangle. The distances between these centers increase with the height-to-base ratio of the triangle (Figure S2A), reflecting the variations of the contributions of their definition parameters (distance to vertex, distance to sides, and distance to the middle of sides). To evaluate centrosome positioning, we fitted a triangular contour to the edges of the plated cytoplast (Figure S2B) to evaluate the position of all centers of the triangles (Figure S2C). With a greater height-to-base ratio, the centrosome was more distant from all pre-defined centers except the geometric center, or center of mass, to which it remained in close proximity (Figures S2D and S2E). This was in agreement with the accepted understanding of centrosome positioning, in that the entire area of the cytoplast, i.e., the entire cell mass, was implicated in its positioning, rather than the cell periphery alone.[10] The robustness of the prediction that the centrosome is positioned at the geometric center was confirmed in cytoplasts plated on more exotic geometries (Figures S3A–S3H).

The centrosome sits at the center of the actin inner zone

Interestingly, we found the centrosome and the geometric center to be separated by a small distance in the cytoplasts plated on short isosceles triangles (Figure 2C), as it was observed in nucleated cells (Figure 1). To further explore the conditions leading to centrosome off-centering, cytoplasts were plated on L-shaped or C-shaped micropattern shapes to impose asymmetric actin network architecture. With both micropatterns, the actin network was asymmetric, and as in the case of nucleated cells, the centrosome was significantly shifted from the geometric center, away from actin transverse arcs and toward peripheral stress fibers (Figure 2D). A similar shift was observed in cytoplast obtained from C2C12 (Figure S3I). This supported the idea that centrosome positioning is affected by the pattern of cell adhesions and the architecture of the actin network, independently of the position of the nucleus.

Interestingly, we noted that a central zone in the cell was devoid of actin bundles, an observation that has been made by others as well,[54] and we termed this region the actin inner zone (AIZ). We manually detected the contour of this zone and its geometrical center: the actin inner center (AIC) (Figure 3A). Our measurements revealed that the centrosome was closer, or equally distant, to the AIC than to the cell geometrical center in all the conditions we tested (Figure 3B; see Figures S4A and S4B for representative examples of centrosome positioning with respect to the AIZ). Therefore, the AIC appeared to be a better descriptor of centrosome positioning than the cell geometrical center

The centrosome position adapts to changes in the architecture of the actin network

The association between the architecture of the actin network and centrosome positioning was further examined by plating cytoplasts on various sizes of disks ranging from 500 to 3,000 μm^2. Surprisingly, we found that the extent of the distribution of centrosome positions was independent of the size of the disk (Figures S4C and S4D). However, the size of the averaged AIZ was also relatively independent of the size of the disk (Figure S4E) in line with the idea that centrosome positioning was sensitive to the AIZ.

To modulate the shape and position of the AIZ, cytoplasts were plated on short isosceles triangles because those shapes were shown to shift centrosome position away from the geometric center (Figure 2C) and because cytoplast spreading was more efficient on triangles than on L or C shapes. Accurate analysis of centrosome positioning was not practical through chemically inhibiting actin assembly, Arp2/3, or formin because of the detachment of cytoplasts from adhesive micropatterns or perturbation of the spreading shape in those conditions. However, inhibiting Rho kinase ROCK with Y27632 resulted in a regular, homogeneous, and homothetic network of thin and loose actin bundles along all cell edges (Figure 4A). In particular, the width of the network along the short edge of the triangle was lower than in the control condition and was similar to those along the two longer edges (Figures 4B and 4C). In cytoplasts treated with the ROCK inhibitor, the center of the AIZ, the AIC, and the centrosome positioned in close proximity to the geometric center, unlike in the control condition, where the AIC and centrosome were positioned further from the short edge of the triangle than the geometric center (Figures 4D and 4E). Noteworthy, in cells displaying a poorly contractile actin network, no transverse arcs and, therefore, no asymmetric AIZ-like PTK2 cells, the centrosome was found precisely at the cell geometrical center (Figure 4F), as in MEF cytoplasts treated with the ROCK inhibitor (Figure 4E). Altogether, these results showed that the actomyosin network acts as a spatial boundary

Figure 3. Centrosome positioning close to the actin inner center (AIC)

(A) Cytoplasts from MEF KO vimentin cells expressing EGFP-Centrin1 were plated on short isosceles triangles, fixed and stained with phalloidin-A555. The scheme shows the analysis performed to study the AIZ and AIC. The red dot represents the geometric centers of the cytoplasts and the green dots the AICs. (B) For a variety of shapes: disks (n = 60), asymmetric disks with border (n = 53), asymmetric disks (n = 43), short isosceles triangles (n = 121), symmetric L (n = 73), asymmetric L (n = 70), and U shape (n = 76). The distance of the centrosome to the cytoplasts geometric center was compared with the distance of the centrosome to the AIC (see Figure S4 for further illustration). The center of the distributions correspond to means. The error bars correspond to the standard error of the mean (SEM). P represents the p value, which was obtained from Mann-Whitney non-parametric tests. Scale bars, 10 μm.

Please cite this article in press as: Jimenez et al., Acto-myosin network geometry defines centrosome position, Current Biology (2021), https://doi.org/10.1016/j.cub.2021.01.002

CellPress

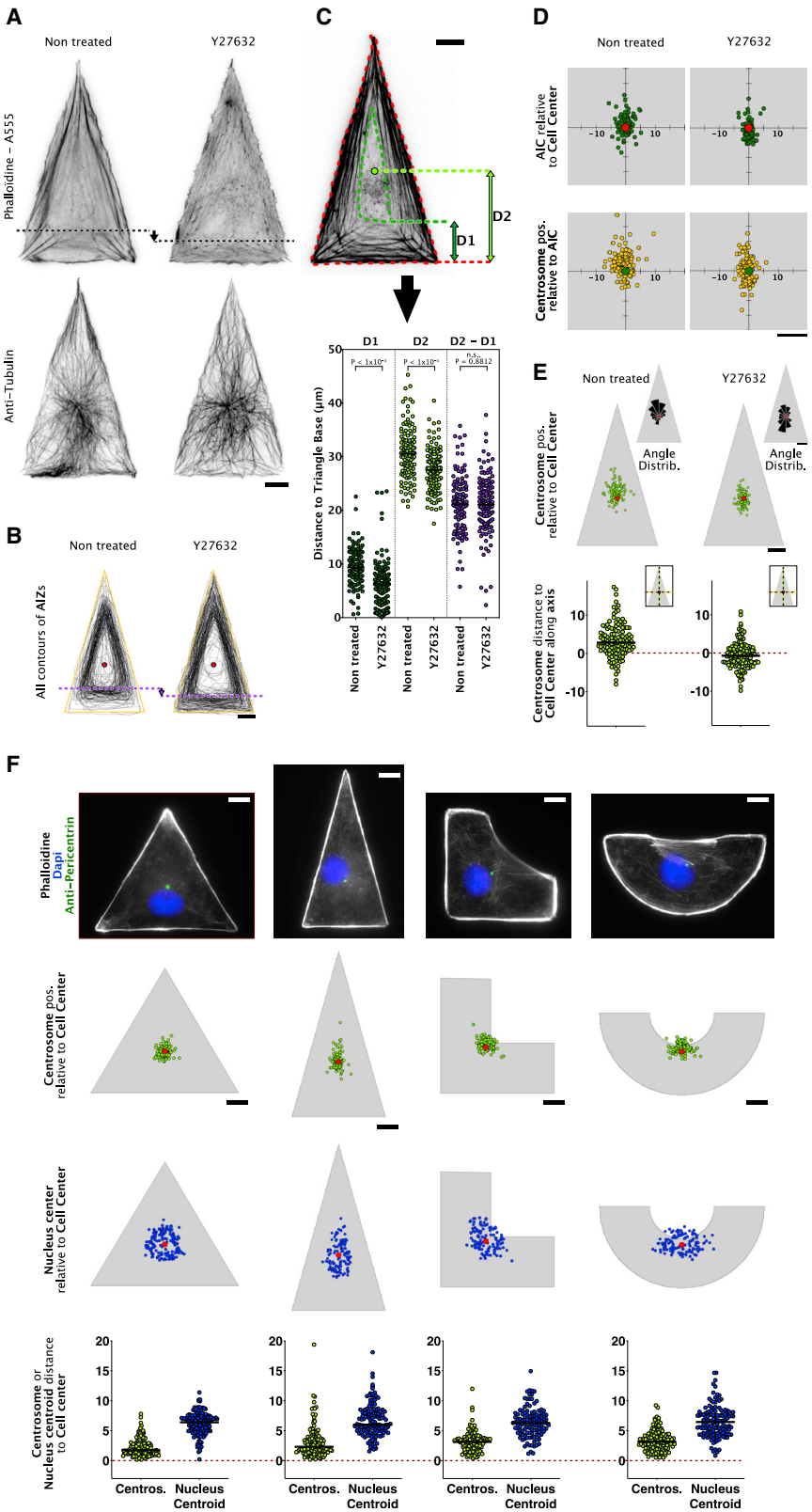

Figure 4. Role of contractility in the architecture of the AIZ and centrosome positioning

Cytoplasts from MEF KO vimentin cells expressing EGFP-Centrin1 were plated on 2,000 µm^2 isosceles "short" triangles for 2 h, then treated for 2 h with Y27632 at 20 µM. Analysis was performed as described before (n = 124 for non-treated; n = 140 for Y27632).

(A) Microtubule and actin staining as in Figure 1. One representative example is given for each condition.

(B) Plots of all the contours of AIZs in relation to the cell center.

(C) The distance from the centrosome to the triangle basis and the distance from the lowest point of the AIZ to the triangle basis (top) were calculated and plotted (bottom) as well as the difference between these two distances.

(D) Plots of all AICs in relation to the cell centroid and of centrosomes in relation to the AIC.

(E) Plots of all centrosomes in relation to the cell center and the respective angle distribution of the population and its distance to cell centroid along indicated axis.

(F) PTK2 cells were platted on isotropic and anisotropic shapes, and for each of them one example is given. The plots show centrosome and nucleus centroid distributions in relation to cell centroid and their distance to cell centroid along the axis indicated by dashed-black arrows. The red dot represents the cell geometrical center, the dark-green dots represents the AIC, and the light-green and yellow dots represent the centrosome. Blue dots represent the nucleus centroid. The dashed red line represents cell centroid position at the graph origin (equilateral, n = 151; isosceles, n = 137; L shape, n = 116; U shape, n = 132). Scale bars, 10 µm.

Please cite this article in press as: Jimenez et al., Acto-myosin network geometry defines centrosome position, Current Biology (2021), https://doi.org/10.1016/j.cub.2021.01.002

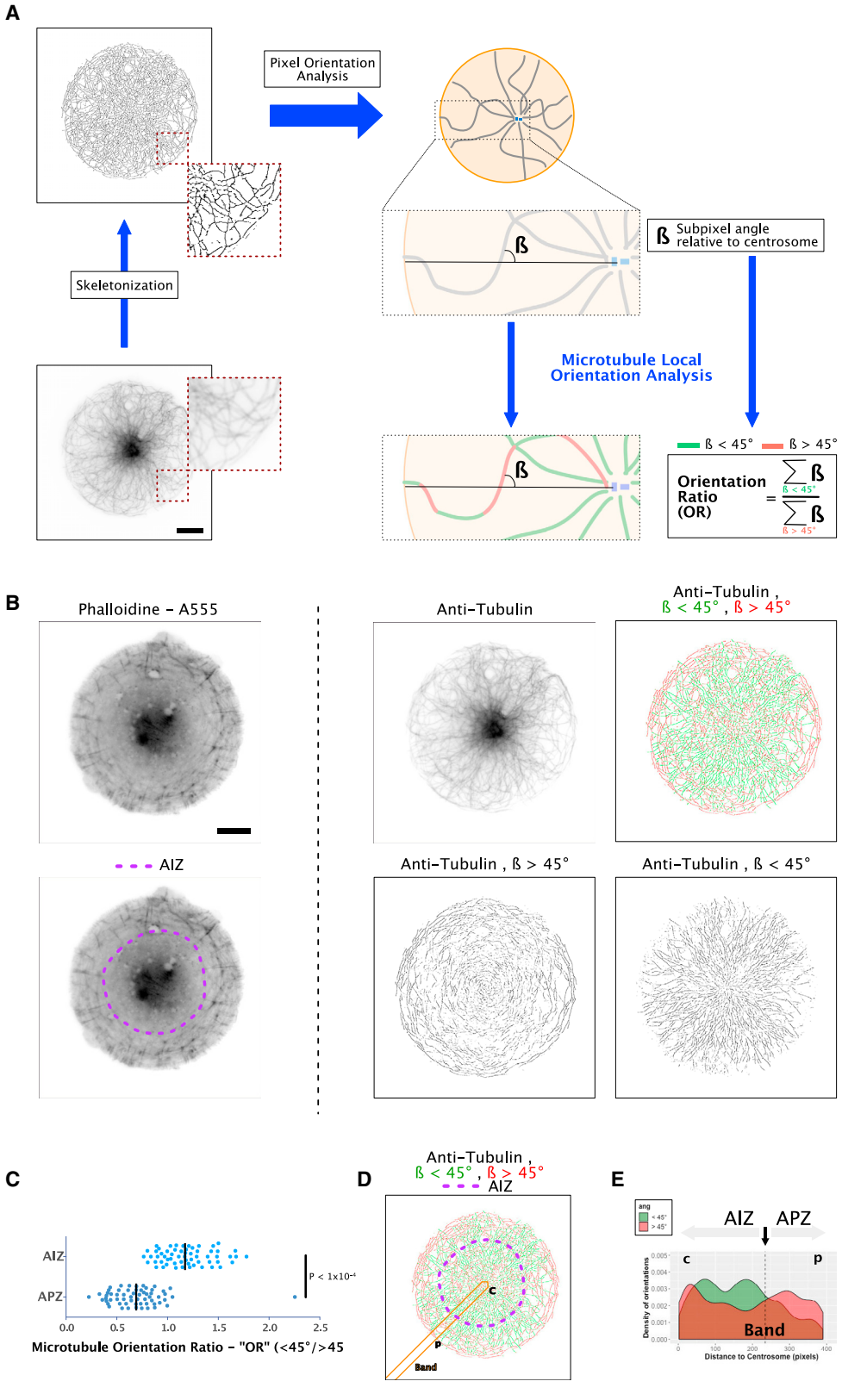

(legend on next page)

Please cite this article in press as: Jimenez et al., Acto-myosin network geometry defines centrosome position, Current Biology (2021), https://doi.org/10.1016/j.cub.2021.01.002

for the microtubule network and thereby affects centrosome position.

Microtubules orientation adapts to the architecture of the actin network

Centrosome positioning is known to depend on the mechanical forces exerted on the microtubule network.[10,14] We thus investigated whether microtubules inside of the AIZ engaged specific and distinct interactions from those on the outside. To quantify how microtubule organization is effected by the AIZ in comparison with the actin-dense region (termed the actin peripheral zone [APZ]), we analyzed local variations in microtubule morphologies and orientations in MEF cytoplasts plated on disc-shaped micropatterns (Figures 5A and 5B) (see examples of segmented networks in Figure S5A). The orientations were clustered into two categories; radial (< 45°) and tangential (> 45°), in relation to the angle in which the microtubule at a given point (pixel) crosses a straight line originating from the centrosome. The averaged local orientation was further described by the orientation ratio, which was defined as the ratio of pixels with radial orientations over those with tangential orientations. Based on orientation ratios, microtubules were more radially oriented in the AIZ than in the APZ (Figure 5C). Moreover, by performing a linescan along a cytoplast radius (Figure 5D), we found that the transition between radial to tangential orientations occurred precisely at the transition between the AIZ and the APZ (Figure 5E; see examples of linescans in Figure S5B). From these results, we concluded that the architecture of the actin network acts locally on the shape and orientation of microtubules.

Microtubule disassembly perturbs centrosome positioning independently of its effect on actin network contractility

Microtubule disassembly is known to impair centrosome positioning.[12,20,32] Cytoplasts were plated on ice (2 h) and treated with 10 μM nocodazole to induce a complete disassembly of microtubules (Figure 6A, middle). As expected, this treatment induced a dispersion of centrosome positions (Figure 6B, middle). However, and in accordance with previous studies, microtubule depletion also increased cell contractility and induced the formation of large actomyosin bundles (Figure 6B, middle).[55,56] The shape of the AIZ was severely deformed and was shifted asymmetrically with respect to the overall cytoplast shape (Figure 6C, middle). The centrosome mis-positioning appeared aligned with the shift of the AIZ (see examples in Figure S6A).

The distortion of the AIZ in response microtubule disassembly could also be detected in cytoplasts plated on disks. Centrosome positioning was not completely random throughout the cytoplast, even after 20 h of nocodazole treatment (Figures S6B and S6C), but limited to the AIZ (Figure S6D). Therefore, and importantly, both experiments suggested that the well-known mispositioning of the centrosome in response to microtubule disassembly resulted not only from the absence of microtubules but also from the deformation of actin-based spatial boundaries through increased actin-network contractility.

To counterbalance the increase of contractility associated to microtubule disassembly, high doses of the ROCK inhibitor Y27632 (100 or 200 μM) were also added to nocodazole-treated cytoplasts (Figure 6A, right). In these conditions, the shape of the AIZ was similar to that in cytoplasts treated with Y27632 alone (at 20 μM); i.e., the AIZ formed a regular, homothetic peripheral band along the cell edges (Figure 6C, right). The lateral shift in the position of the AIZ was less than that in cytoplasts treated with nocodazole alone and the distribution of centrosomes followed the same trend (Figure 6B). Notably, in response to either nocodazole alone or nocodazole and Y27632, the centrosome-AIC distances were higher than those in the control cytoplasts (Figure 6D), showing that although centrosome positioning was coordinated with AIZ displacement, centrosomes were dispersed within the AIZ in the absence of microtubules. This suggested that microtubules direct centrosome positioning to the center of the AIZ.

Dyneins position the centrosome at the center of the actin inner zone

Dyneins have been shown to be involved in centrosome positioning in eggs,[16] embryos,[13,57] unicellular eukaryotes,[15,58,59] and mammalian cells.[12,14] The two dynein inhibitors we tested, ciliobrevin D and dynarrestin, had no clear effect on the dispersion of the Golgi apparatus, which is a classic readout for dynein inactivation. Therefore, we chose to inhibit dynein activity by expressing a dominant-negative form of the dynactin subunit p150 glued (p150-DN).[60] For these experiments, we worked with WT MEFs to detect the GFP signal of p150-DN without being perturbed by the centrin1-GFP signal in the vimentin-KO line used before. In cytoplast of WT MEFs plated on isoceles triangle, the centrosome was off-centered in relation to cell geometrical center as in vimentin-KO cytoplasts (Figures S7C and S7D). In dynein-inactivated cytoplasts, the centrosomes were more dispersed than in control cytoplasts but still biased toward the apex of the triangle and the position of the AIZ (Figure 7A). Similar observations were made upon dynein inactivation in RPE1 cytoplasts (Figures S7A and S7B). In these conditions, microtubules were curvy all over the cell (Figure 7B), and the networks were highly asymmetric (Figures S7A and S7B). However, the position of the centrosome

Figure 5. Analysis of microtubule orientation in and outside the AIZ

Cytoplasts from MEF KO vimentin cells expressing EGFP-Centrin1 were plated on 2,000 μm^2 disks and stained for actin and microtubules as in Figure 1.

(A) Overview of the microtubule network analysis. The orientation ratio or "OR" is the ratio of the number of non-null pixels with an orientation < 45°C and the number of non-null pixels with an orientation > 45°C.

(B) Example of analyzed cytoplast (see Figure S5A for more examples).

(C) Overview of the microtubule-AIZ cross-analysis: microtubule network analysis was performed along a radial band and in the AIZ and in the APZ (n = 60). The center of the distributions correspond to medians. P represents p value, which was obtained from a Mann-Whitney non-parametric test.

(D) Results of cross-analysis plotting the analysis: microtubule network analysis was performed along a radial band, and the ones outside the AIZ (in the APZ) are preferentially oriented tangentially.

(E) The independently determined AIZ boundary matches the boundary of two zones defined by a clear majority of radial or tangential microtubules, respectively (see Figure S5B for examples). Scale bars, 10 μm.

Please cite this article in press as: Jimenez et al., Acto-myosin network geometry defines centrosome position, Current Biology (2021), https://doi.org/10.1016/j.cub.2021.01.002

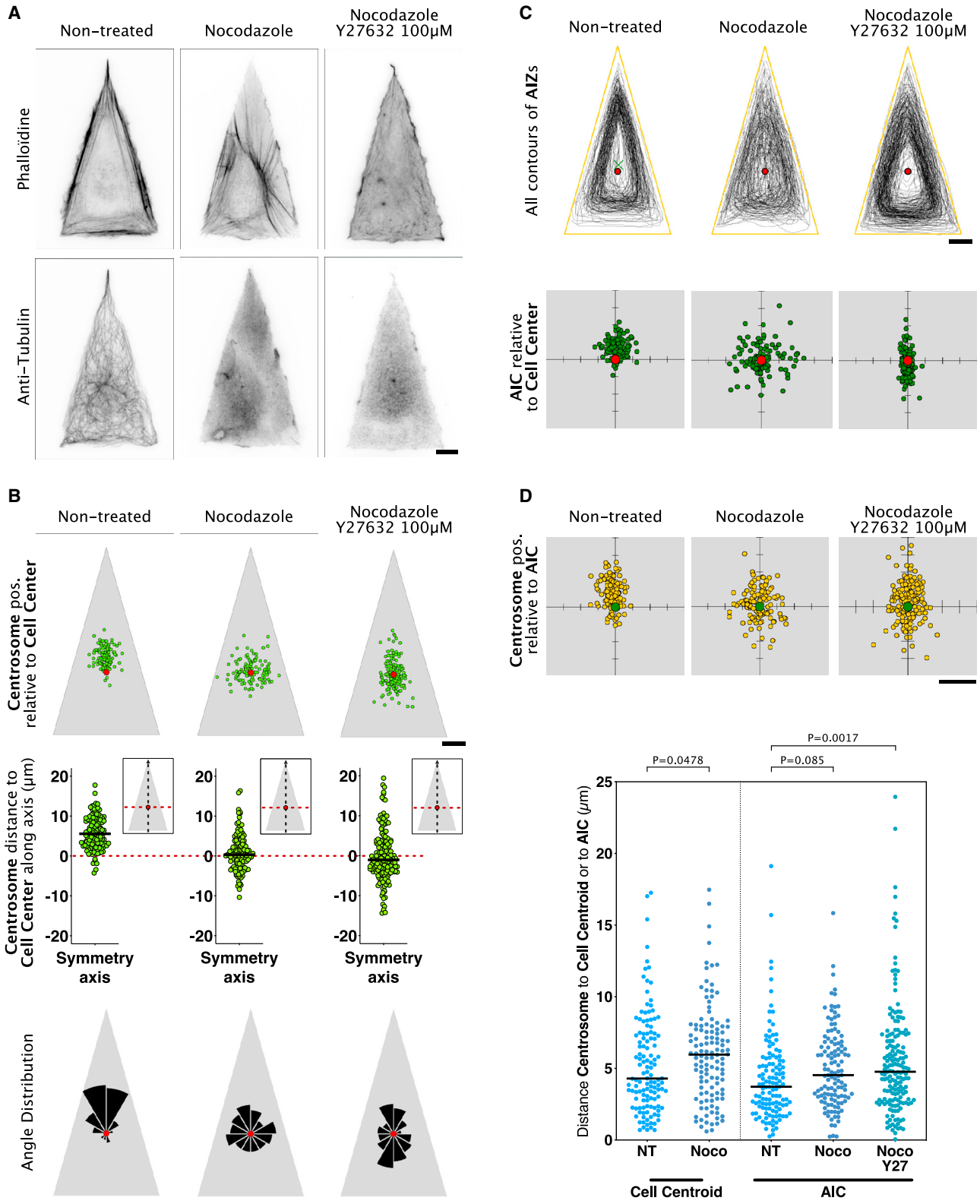

Figure 6. Effect of microtubule disassembly on AIZ and centrosome positioning

Cytoplasts from MEF KO Vimentin cells expressing EGFP-Centrin1 plated on 2,000 μm^2 isosceles "short" triangles were treated with Ice-Nocodazole 10 µM or Ice-Nocodazole 10 µM and Y27632 100 µM in order to uncouple the effect of contractility and the one of microtubules depletion (non-treated, n = 121; nocodazole, n = 120; nocodazole and Y27632, n = 170).

(legend continued on next page)

Please cite this article in press as: Jimenez et al., Acto-myosin network geometry defines centrosome position, Current Biology (2021), https://doi.org/10.1016/j.cub.2021.01.002

remained limited by the actin bundles (Figure 7B), suggesting that dyneins were involved in centrosome positioning with respect to this network.

To further test this hypothesis, we used the same experimental strategy as before to annihilate actin contractile network asymmetry by relaxing acto-myosin contractility. In dynein-inactivated cytoplasts treated with the ROCK inhibitor Y27632, centrosomes were then dispersed all over the cell and around the geometric center, corresponding to the shifted position of the AIZ (see the positions and angular distributions of centrosome in Figure 7A, second and fourth columns). This showed that dyneins directed centrosome positioning to the center of the AIZ rather than to the geometric center of the cell.

To better understand how dyneins could direct centrosome position at the center of the AIZ, we performed a co-labeling of actin filaments, microtubules, and p150 glued (Figure 7C). Dynein labeling revealed that dyneins were not evenly distributed throughout the entire cell and were concentrated within the AIZ (Figure 7D). This suggested that, in addition to the peripheral pushing forces exerted by contractile actin bundles deforming microtubules out of the AIZ (Figure 5), microtubules were put under higher tension in the AIZ by the concentrated distribution of dyneins in this region.

DISCUSSION

Centrosome, nucleus, and the cell geometrical center

The mechanism that specifically regulates the positioning of the centrosome in mammalian cells has long been confused with the mechanism that regulates the position of the nucleus, and notably the actomyosin network acting on the nucleus.[28,36,42] The consensus has been that the centrosome positions at the cell's geometric center, either autonomously[23,32] or in association with the nucleus.[20] Here, we established an *in vitro* cell system to study centrosome positioning in which a number of parameters were controlled. This system included cytoplasts devoid of nuclei and the major intermediate filament, vimentin, and cytoplasts of defined shapes dictated by the micropatterned substrates onto which they were plated. We showed that the centrosome position is defined by the architecture of the actin network. More precisely, it is positioned at the geometric center of an inner space that is devoid of actin bundles. This position can correspond or not to the geometric center of the cell, depending on the anisotropy of the actin network, which in turn responds to the spatial distribution of cell adhesions.

Furthermore, our experiments in nucleated cells showed that centrosome off-centering is also active in cells but that it can be perturbed by the mechanism of nucleus positioning. In poorly contractile cells like PTK2, the centrosome distribution was well clustered around cell geometrical center and the nucleus distribution was spread around it (Figure 4). By contrast, in more contractile cells like fibroblasts, RPE1 cells, or C2C12 myoblasts, the distribution of centrosomes were more dispersed than the distribution of nuclei (Figures S1A and S1B), and the distribution of centrosomes were more clustered in cytoplast than in cells (Figure S3I), suggesting that the nucleus position is strongly determined by the contraction of the acto-myosin network and that the nucleus can displace the centrosome from its position at the center of the actin inner zone. These data showed that both organelles have independent self-centering properties[4,34] and that the level of acto-myosin contraction defines which of the two will dominate the competition.

Microtubule and actin

Microtubules interact with actin via specific crosslinkers or non-specific steric interactions.[61] In particular, a dense and growing actin network can apply pushing forces on microtubules.[62,63] Here, we found that the actomyosin network constitutes the actual spatial boundary to which the microtubules are sensitive. Disrupting or modifying the geometry of the actin network via the pattern of cell adhesions, altered the spatial boundary and changed centrosome position accordingly (Figures 2, 3, and 4). Microtubules appeared more bent within the actomyosin network at the cell periphery, and straighter in the central part devoid of actin (Figure 5). These results suggested that centrosome positioning is mainly ensured by a combination of peripheral pushing and central pulling forces along microtubules.

Dyneins

Dynein have long been known to apply pulling forces on microtubules and to be thus involved in MTOC positioning. By acting at the periphery or throughout the cytoplasm in round eggs, dyneins are thought to position the centrosome at the egg geometrical center.[10] We found here that in adherent mammalian cells, the activity of dynein is not evenly distributed all over cell periphery but rather restricted to specific regions of the cell cortex. Indeed, the linear shape and radial orientation of microtubules and the increased amount of dynein within the central part of the basal cortex devoided of actin bundles suggest that dyneins put microtubules under tension in a subcellular pattern defined by the geometry of the contractile actin network (Figures 4B–4E, 7C, and S5B). Consistent with this view, the microtubules are not able to interact with cell periphery in aged cytoplasts but the centrosome remains well positioned, suggesting that the inner part of the cell cortex is sufficient to ensure centrosome position at the cell center.[64] Dynein activity requires dynactin to be coupled to a cargo or any other substrate supporting the force

(A) Representative images of cytoplasts from both conditions (see Figure S6 for more examples). In the absence of microtubules, actin contractility is highly increased. In cells depleted for microtubules and treated with Y27632 at 20 μM, contractility was still abnormally high (not shown). A higher concentration of Y27632 (100–200 μM) was then used. As observed in the example cell, this concentration was sufficient to inhibit contractility in the absence of microtubules.
(B) Plots of all centrosomes in relation to the cell center, distance to cell centroid along indicated axis, and the angle distribution of the population.
(C) Plots of all the contours of AICs in relation to the cell centroid and of centrosomes in relation to the AIC.
(D) The top panel plots of all AICs in relation to the cell centroid and of centrosomes in relation to the AIC. The bottom panel is the plot of the distance between the centrosome and the cell centroid or the AIC for the indicated conditions. Red dots represent the cell geometrical center and dark-green dots represent the AIC. The light-green and yellow dots represent the centrosome. The center of the distributions correspond to medians. P represents p value, which was obtained from Mann-Whitney non-parametric tests. Scale bars, 10 μm.

Please cite this article in press as: Jimenez et al., Acto-myosin network geometry defines centrosome position, Current Biology (2021), https://doi.org/10.1016/j.cub.2021.01.002

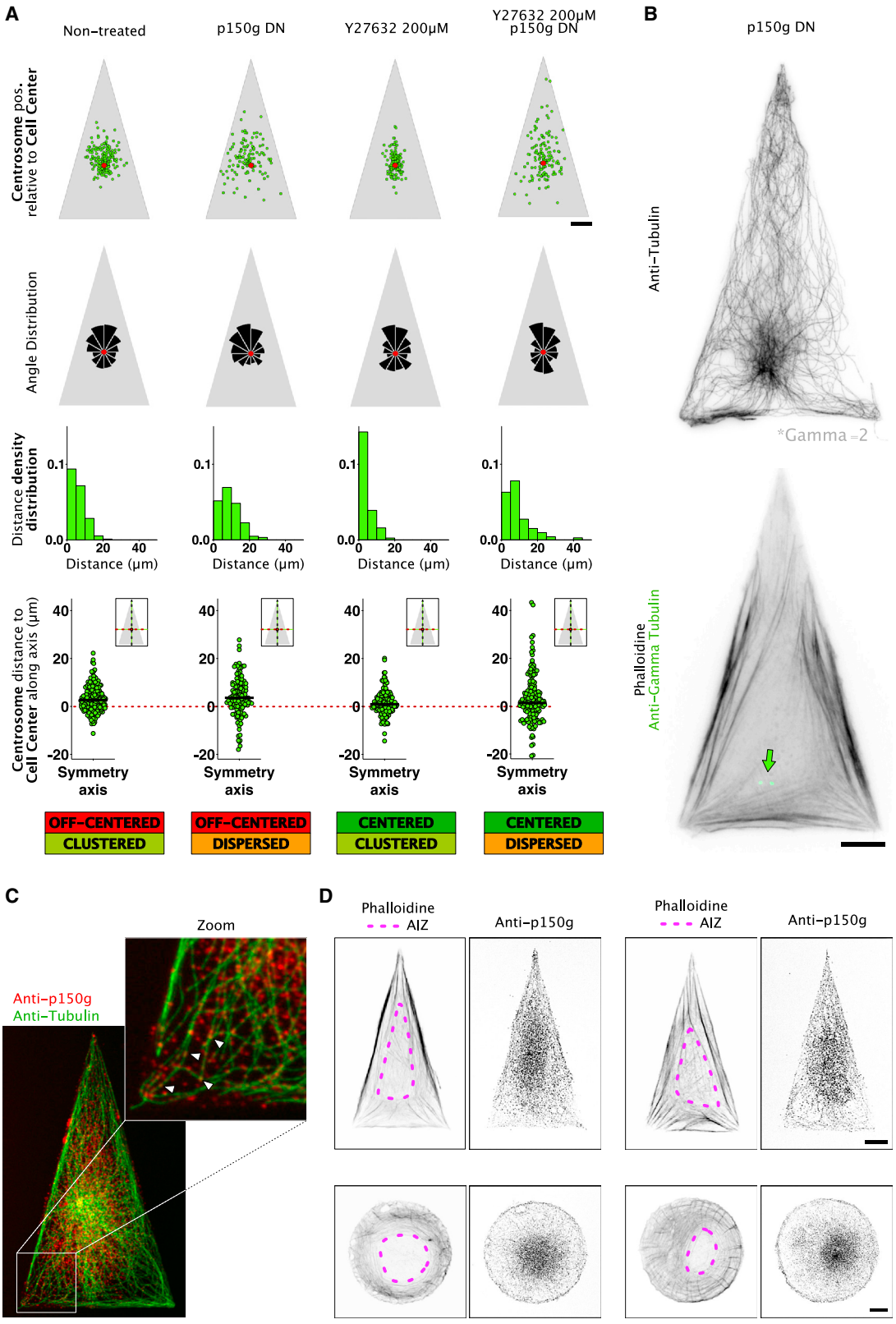

(legend on next page)

load. In large and round embryos, dyneins have been proposed to act as a coupling device that transmits contractile forces from the actomyosin network onto microtubules.[57] Whether this applies to spread cells, and how it sets and organizes tensional forces in these conditions, remains to be investigated.

Implications for centrosome positioning in differentiated and polarized cells

The centrosome-positioning forces mediated via the actin network appeared potent and relevant for the cell *in vivo* because highly asymmetric actin networks, such as those developed on C-shaped micropatterns, brought the centrosome into contact with cell periphery, potentially reflecting the peripheral positioning mechanism in migrating or polarized cells.[1,2] Therefore, a change in actin contractility and actin-network asymmetry (due to changes in adhesion geometry) could be the initial step affecting the organization of microtubules and the distribution of dyneins, which, by repositioning the centrosome, could further bias internal traffic and reinforce the directional bias of the cell's polarization.

STAR★METHODS

Detailed methods are provided in the online version of this paper and include the following:

- KEY RESOURCES TABLE
- RESOURCE AVAILABILITY
  - Lead contact
  - Materials Availability
  - Data and Code Availability
- EXPERIMENTAL MODEL AND SUBJECT DETAILS
  - Cell lines
  - Cell Culture
- METHOD DETAILS
  - Enucleation
  - Drug treatment
  - Fixation and Immunostaining
  - Micropatterning
  - Imaging
  - Centrosome positioning compared triangle characteristic centers
  - Actin inner zone (AIZ) and actin inner center (AIC)
  - Dot plots and plots of AIZs
  - Microtubule orientations
- QUANTIFICATION AND STATISTICAL ANALYSIS

SUPPLEMENTAL INFORMATION

Supplemental Information can be found online at https://doi.org/10.1016/j.cub.2021.01.002.

ACKNOWLEDGMENTS

We thank Robert Goldman and John Eriksson for sharing the MEF WT and vimentin-KO cell lines; Andrew Holland for sharing RPE1 puromycin sensitive cells; Hiroki Umeshima for sending us the plasmid p150 glued DN; Franck Perez, Sandrine Moutel, and the plateform TabIP for sharing their electroporator and antibodies; the cytometry platform of the Institute for Research of Saint-Louis Hospital; and Tanguy Chocat and Esteban Beuve Helissey for their assistance in performing experiments. We thank Franck Perez for allowing A.J.J. time for revision experiments. This work was supported by the European Research Council (ERC Adv 741773 to L.B. and ERC CoG 771599 to M.T.) and a post-doctoral fellowship from La Ligue contre le cancer (FFJL14157 to A.J.J.).

AUTHOR CONTRIBUTIONS

Conceptualization: M.T., L.B., M.P., M.B., and A.J.J.; funding acquisition, M.T., L.B., and A.J.J.; methodology: M.T., L.B., A.J.J., M.P., M.B., and A.S.; investigation: A.J.J., A.S., C.D., G.L., and B.V.; analysis: M.T., L.B., A.J.J., and G.L.; supervision: M.T. and L.B. Writing: M.T. and A.J.J.

DECLARATION OF INTERESTS

The authors declare no conflict of interest.

Received: February 19, 2020
Revised: November 20, 2020
Accepted: January 4, 2021
Published: February 19, 2021

REFERENCES

1. Tang, N., and Marshall, W.F. (2012). Centrosome positioning in vertebrate development. J. Cell Sci. *125*, 4951–4961.
2. Bornens, M. (2018). Cell polarity: having and making sense of direction-on the evolutionary significance of the primary cilium/centrosome organ in Metazoa. Open Biol. *8*, 180052.
3. Burakov, A.V., and Nadezhdina, E.S. (2020). Centering and Shifting of Centrosomes in Cells. Cells *9*, 1351.
4. Vallee, R.B., and Stehman, S.A. (2005). How dynein helps the cell find its center: a servomechanical model. Trends Cell Biol. *15*, 288–294.
5. Sanchez, A.D., and Feldman, J.L. (2016). Microtubule-organizing centers: from the centrosome to non-centrosomal sites. Curr. Opin. Cell Biol. *44*, 1–9.
6. Pitaval, A., Senger, F., Letort, G., Gidrol, X., Guyon, L., Sillibourne, J., and Théry, M. (2017). Microtubule stabilization drives 3D centrosome migration to initiate primary ciliogenesis. J. Cell Biol. *216*, 3713–3728.

Figure 7. Role of dyneins in centrosome positioning in the AIZ

Cytoplasts of MEF WT cells electroporated with p150-DN 48 h before enucleation, and positive cells were sorted by flow cytometry 24 h before enucleation. Cytoplasts were plated on 2,000 μm^2 isosceles "short" for 2 h and treated when indicated with Y27632 at 200 μM for 2 extra h (non-treated, n = 190; p150 gDN, n = 124; Y27632, n = 164; p150 gDN/Y27632, n = 146)

(A) First line shows the plots of all centrosomes in relation to the cell center. The second line shows the respective angle distribution. The third line shows the density distribution of the centrosome-cell centroid distance, and the fourth line shows the centrosome-cell centroid distance along the axis indicated by dashed black arrows. The red dashed line represents the cell centroid position at the origin of the graph. See Figure S7A for similar experiments using RPE1 cytoplasts.

(B) Example of centrosome off-centering in p150 g-DN transfected cell. Red dots represent cell geometrical center and light green dots represent the centrosome. Green arrow points at the centrosome.

(C) Co-staining for microtubules and dyneins. Arrow heads point at dynein dots co-localizing with microtubules.

(D) Examples of cytoplasts stained for actin and for dynein by using anti-p150 glued antibodies. The images were processed with an unsharp mask for better visualization. The AIZ was determined and represented by purple dashed lines. The maximum projection of the dynein images shows a higher overall amount of dynein inside the AIZ. This illustrated by scan lines presented in Figures S7E and S7F. Scale bars, 10μm.

7. Shao, W., Yang, J., He, M., Yu, X.Y., Lee, C.H., Yang, Z., Joyner, A.L., Anderson, K.V., Zhang, J., Tsou, M.B., et al. (2020). Centrosome anchoring regulates progenitor properties and cortical formation. Nature *580*, 106–112.
8. Stinchcombe, J.C., and Griffiths, G.M. (2014). Communication, the centrosome and the immunological synapse. Philos. Trans. R. Soc. Lond. B Biol. Sci. *369*, 20130463.
9. Burute, M., Prioux, M., Blin, G., Truchet, S., Letort, G., Tseng, Q., Bessy, T., Lowell, S., Young, J., Filhol, O., and Théry, M. (2017). Polarity Reversal by Centrosome Repositioning Primes Cell Scattering during Epithelial-to-Mesenchymal Transition. Dev. Cell *40*, 168–184.
10. Kimura, K., and Kimura, A. (2011). A novel mechanism of microtubule length-dependent force to pull centrosomes toward the cell center. Bioarchitecture *1*, 74–79.
11. Zhu, J., Burakov, A., Rodionov, V., and Mogilner, A. (2010). Finding the cell center by a balance of dynein and myosin pulling and microtubule pushing: a computational study. Mol. Biol. Cell *21*, 4418–4427.
12. Burakov, A., Nadezhdina, E., Slepchenko, B., and Rodionov, V. (2003). Centrosome positioning in interphase cells. J. Cell Biol. *162*, 963–969.
13. Nguyen-Ngoc, T., Afshar, K., and Gönczy, P. (2007). Coupling of cortical dynein and G alpha proteins mediates spindle positioning in Caenorhabditis elegans. Nat. Cell Biol. *9*, 1294–1302.
14. Wu, J., Misra, G., Russell, R.J., Ladd, A.J.C., Lele, T.P., and Dickinson, R.B. (2011). Effects of dynein on microtubule mechanics and centrosome positioning. Mol. Biol. Cell *22*, 4834–4841.
15. Koonce, M.P., Köhler, J., Neujahr, R., Schwartz, J.M., Tikhonenko, I., and Gerisch, G. (1999). Dynein motor regulation stabilizes interphase microtubule arrays and determines centrosome position. EMBO J. *18*, 6786–6792.
16. Tanimoto, H., Kimura, A., and Minc, N. (2016). Shape-motion relationships of centering microtubule asters. J. Cell Biol. *212*, 777–787.
17. Brito, D.A., Strauss, J., Magidson, V., Tikhonenko, I., Khodjakov, A., and Koonce, M.P. (2005). Pushing forces drive the comet-like motility of microtubule arrays in Dictyostelium. Mol. Biol. Cell *16*, 3334–3340.
18. Garzon-Coral, C., Fantana, H.A., and Howard, J. (2016). A force-generating machinery maintains the spindle at the cell center during mitosis. Science *352*, 1124–1127.
19. Pinot, M., Chesnel, F., Kubiak, J.Z., Arnal, I., Nedelec, F.J., and Gueroui, Z. (2009). Effects of confinement on the self-organization of microtubules and motors. Curr. Biol. *19*, 954–960.
20. Hale, C.M., Chen, W.-C., Khatau, S.B., Daniels, B.R., Lee, J.S.H., and Wirtz, D. (2011). SMRT analysis of MTOC and nuclear positioning reveals the role of EB1 and LIC1 in single-cell polarization. J. Cell Sci. *124*, 4267–4285.
21. Chevrier, V., Piel, M., Collomb, N., Saoudi, Y., Frank, R., Paintrand, M., Narumiya, S., Bornens, M., and Job, D. (2002). The Rho-associated protein kinase p160ROCK is required for centrosome positioning. J. Cell Biol. *157*, 807–817.
22. Théry, M., Racine, V., Piel, M., Pépin, A., Dimitrov, A., Chen, Y., Sibarita, J.-B., and Bornens, M. (2006). Anisotropy of cell adhesive microenvironment governs cell internal organization and orientation of polarity. Proc. Natl. Acad. Sci. USA *103*, 19771–19776.
23. Graham, D.M., Andersen, T., Sharek, L., Uzer, G., Rothenberg, K., Hoffman, B.D., Rubin, J., Balland, M., Bear, J.E., and Burridge, K. (2018). Enucleated cells reveal differential roles of the nucleus in cell migration, polarity, and mechanotransduction. J. Cell Biol. *217*, 895–914.
24. Laan, L., Pavin, N., Husson, J., Romet-Lemonne, G., van Duijn, M., López, M.P., Vale, R.D., Jülicher, F., Reck-Peterson, S.L., and Dogterom, M. (2012). Cortical dynein controls microtubule dynamics to generate pulling forces that position microtubule asters. Cell *148*, 502–514.
25. Letort, G., Nedelec, F., Blanchoin, L., and Théry, M. (2016). Centrosome centering and decentering by microtubule network rearrangement. Mol. Biol. Cell *27*, 2833–2843.
26. Pavin, N., Laan, L., Ma, R., Dogterom, M., and Jülicher, F. (2012). Positioning of microtubule organizing centers by cortical pushing and pulling forces. New J. Physiol. *14*, https://doi.org/10.1088/1367-2630/14/10/105025.
27. Pouthas, F., Girard, P., Lecaudey, V., Ly, T.B.N., Gilmour, D., Boulin, C., Pepperkok, R., and Reynaud, E.G. (2008). In migrating cells, the Golgi complex and the position of the centrosome depend on geometrical constraints of the substratum. J. Cell Sci. *121*, 2406–2414.
28. Luxton, G.W.G., and Gundersen, G.G. (2011). Orientation and function of the nuclear-centrosomal axis during cell migration. Curr. Opin. Cell Biol. *23*, 579–588.
29. Zhang, J., and Wang, Y. (2017). Centrosome defines the rear of cells during mesenchymal migration. Mol. Biol. Cell *28*, https://doi.org/10.1091/mbc.e17-06-0366.
30. Rodríguez-Fraticelli, A.E., Auzan, M., Alonso, M.A., Bornens, M., and Martín-Belmonte, F. (2012). Cell confinement controls centrosome positioning and lumen initiation during epithelial morphogenesis. J. Cell Biol. *198*, 1011–1023.
31. Gomes, E.R., Jani, S., and Gundersen, G.G. (2005). Nuclear movement regulated by Cdc42, MRCK, myosin, and actin flow establishes MTOC polarization in migrating cells. Cell *121*, 451–463.
32. Dupin, I., Camand, E., and Etienne-Manneville, S. (2009). Classical cadherins control nucleus and centrosome position and cell polarity. J. Cell Biol. *185*, 779–786.
33. Dupin, I., and Etienne-Manneville, S. (2011). Nuclear positioning: mechanisms and functions. Int. J. Biochem. Cell Biol. *43*, 1698–1707.
34. Reinsch, S., and Gönczy, P. (1998). Mechanisms of nuclear positioning. J. Cell Sci. *111*, 2283–2295.
35. Bornens, M. (1977). Is the centriole bound to the nuclear membrane? Nature *270*, 80–82.
36. Burakov, A.V., and Nadezhdina, E.S. (2013). Association of nucleus and centrosome: magnet or velcro? Cell Biol. Int. *37*, 95–104.
37. Salpingidou, G., Smertenko, A., Hausmanowa-Petrucewicz, I., Hussey, P.J., and Hutchison, C.J. (2007). A novel role for the nuclear membrane protein emerin in association of the centrosome to the outer nuclear membrane. J. Cell Biol. *178*, 897–904.
38. Zhang, X., Lei, K., Yuan, X., Wu, X., Zhuang, Y., Xu, T., Xu, R., and Han, M. (2009). SUN1/2 and Syne/Nesprin-1/2 complexes connect centrosome to the nucleus during neurogenesis and neuronal migration in mice. Neuron *64*, 173–187.
39. Malone, C.J., Misner, L., Le Bot, N., Tsai, M.C., Campbell, J.M., Ahringer, J., and White, J.G. (2003). The C. elegans hook protein, ZYG-12, mediates the essential attachment between the centrosome and nucleus. Cell *115*, 825–836.
40. Biedzinski, S., Agsu, G., Vianay, B., Delord, M., Blanchoin, L., Larghero, J., Faivre, L., Théry, M., and Brunet, S. (2020). Microtubules control nuclear shape and gene expression during early stages of hematopoietic differentiation. EMBO J. *39*, e103957.
41. Starr, D.A., and Fridolfsson, H.N. (2010). Interactions between nuclei and the cytoskeleton are mediated by SUN-KASH nuclear-envelope bridges. Annu. Rev. Cell Dev. Biol. *26*, 421–444.
42. Burke, B., and Roux, K.J. (2009). Nuclei take a position: managing nuclear location. Dev. Cell *17*, 587–597.
43. Karsenti, E., Kobayashi, S., Mitchison, T., and Kirschner, M. (1984). Role of the centrosome in organizing the interphase microtubule array: properties of cytoplasts containing or lacking centrosomes. J. Cell Biol. *98*, 1763–1776.
44. Umeshima, H., Hirano, T., and Kengaku, M. (2007). Microtubule-based nuclear movement occurs independently of centrosome positioning *104*, 16182–16187.
45. Strzyz, P.J., Lee, H.O., Sidhaye, J., Weber, I.P., Leung, L.C., and Norden, C. (2015). Interkinetic nuclear migration is centrosome independent and ensures apical cell division to maintain tissue integrity. Dev. Cell *32*, 203–219.

46. Théry, M., Pépin, A., Dressaire, E., Chen, Y., and Bornens, M. (2006). Cell distribution of stress fibres in response to the geometry of the adhesive environment. Cell Motil. Cytoskeleton *63*, 341–355.

47. Chen, T., Callan-Jones, A., Fedorov, E., Ravasio, A., Brugués, A., Ong, H.T., Toyama, Y., Low, B.C., Trepat, X., Shemesh, T., et al. (2019). Large-scale curvature sensing by directional actin flow drives cellular migration mode switching. Nat. Phys. *15*, 393–402.

48. Mandal, K., Wang, I., Vitiello, E., Orellana, L.A.C., and Balland, M. (2014). Cell dipole behaviour revealed by ECM sub-cellular geometry. Nat. Commun. *5*, 5749.

49. Piel, M., Meyer, P., Khodjakov, A., Rieder, C.L., and Bornens, M. (2000). The respective contributions of the mother and daughter centrioles to centrosome activity and behavior in vertebrate cells. J. Cell Biol. *149*, 317–330.

50. Patteson, A.E., Vahabikashi, A., Pogoda, K., Adam, S.A., Mandal, K., Kittisopikul, M., Sivagurunathan, S., Goldman, A., Goldman, R.D., and Janmey, P.A. (2019). Vimentin protects cells against nuclear rupture and DNA damage during migration. J. Cell Biol. *218*, 4079–4092.

51. Cheng, F., Shen, Y., Mohanasundaram, P., Lindström, M., Ivaska, J., Ny, T., and Eriksson, J.E. (2016). Vimentin coordinates fibroblast proliferation and keratinocyte differentiation in wound healing via TGF-β-Slug signaling. Proc. Natl. Acad. Sci. USA *113*, E4320–E4327.

52. Mendez, M.G., Kojima, S., and Goldman, R.D. (2010). Vimentin induces changes in cell shape, motility, and adhesion during the epithelial to mesenchymal transition. FASEB J. *24*, 1838–1851.

53. Kimberling, C.. Encyclopedia of Triangle Centers. https://faculty.evansville.edu/ck6/encyclopedia/etc.html.

54. Dong, L., Gong, J., Wang, Y., He, J., You, D., Zhou, Y., Li, Q., Liu, Y., Cheng, K., Qian, J., et al. (2019). Chiral geometry regulates stem cell fate and activity. Biomaterials *222*, 119456.

55. Krendel, M., Zenke, F.T., and Bokoch, G.M. (2002). Nucleotide exchange factor GEF-H1 mediates cross-talk between microtubules and the actin cytoskeleton. Nat. Cell Biol. *4*, 294–301.

56. Chang, Y.C., Nalbant, P., Birkenfeld, J., Chang, Z.F., and Bokoch, G.M. (2008). GEF-H1 couples nocodazole-induced microtubule disassembly to cell contractility via RhoA. Mol. Biol. Cell *19*, 2147–2153.

57. De Simone, A., Nédélec, F., and Gönczy, P. (2016). Dynein Transmits Polarized Actomyosin Cortical Flows to Promote Centrosome Separation. Cell Rep. *14*, 2250–2262.

58. Rehberg, M., Kleylein-Sohn, J., Faix, J., Ho, T.-H., Schulz, I., and Gräf, R. (2005). Dictyostelium LIS1 is a centrosomal protein required for microtubule/cell cortex interactions, nucleus/centrosome linkage, and actin dynamics. Mol. Biol. Cell *16*, 2759–2771.

59. Vogel, S.K., Pavin, N., Maghelli, N., Jülicher, F., and Tolić-Nørrelykke, I.M. (2009). Self-organization of dynein motors generates meiotic nuclear oscillations. PLoS Biol. *7*, e1000087.

60. Wu, Y.K., Umeshima, H., Kurisu, J., and Kengaku, M. (2018). Nesprins and opposing microtubule motors generate a point force that drives directional nuclear motion in migrating neurons. Development *145*, 1–10.

61. Dogterom, M., and Koenderink, G.H. (2018). Actin–microtubule crosstalk in cell biology. Nat. Rev. Mol. Cell Biol. *1*, 38–54.

62. Colin, A., Singaravelu, P., Théry, M., Blanchoin, L., and Gueroui, Z. (2018). Actin-Network Architecture Regulates Microtubule Dynamics. Curr. Biol. *28*, 2647–2656.e4.

63. Gupton, S.L., Salmon, W.C., and Waterman-Storer, C.M. (2002). Converging populations of f-actin promote breakage of associated microtubules to spatially regulate microtubule turnover in migrating cells. Curr. Biol. *12*, 1891–1899.

64. Brodsky, I.B., Burakov, A.V., and Nadezhdina, E.S. (2007). Microtubules' interaction with cell cortex is required for their radial organization, but not for centrosome positioning. Cell Motil. Cytoskeleton *64*, 407–417.

65. Colucci-Guyon, E., Portier, M.M., Dunia, I., Paulin, D., Pournin, S., and Babinet, C. (1994). Mice lacking vimentin develop and reproduce without an obvious phenotype. Cell *79*, 679–694.

66. Stuurman, N., Edelstein, A.D., Amodaj, N., Hoover, K.H., and Vale, R.D. (2010). Computer Control of Microscopes using mManager. Curr. Protoc. Mol. Biol. Ed. Frederick M Ausubel Al Chapter 14: Unit14.20

67. Strale, P.O., Azioune, A., Bugnicourt, G., Lecomte, Y., Chahid, M., and Studer, V. (2016). Multiprotein Printing by Light-Induced Molecular Adsorption. Adv. Mater. *28*, 2024–2029.

68. Azioune, A., Carpi, N., Tseng, Q., Théry, M., and Piel, M. (2010). Protein micropatterns: A direct printing protocol using deep UVs. Methods Cell Biol. *97*, 133–146.

69. Schneider, C.A., Rasband, W.S., and Eliceiri, K.W. (2012). NIH Image to ImageJ: 25 years of image analysis. Nat. Methods *9*, 671–675.

Please cite this article in press as: Jimenez et al., Acto-myosin network geometry defines centrosome position, Current Biology (2021), https://doi.org/10.1016/j.cub.2021.01.002

STAR★METHODS

KEY RESOURCES TABLE

REAGENT or RESOURCE	SOURCE	IDENTIFIER
Antibodies		
Anti-Tubulin	Abd serotec	MCA77G; RRID: AB_325003
Anti-Tubulin	Abcam	ab18251; RRID: AB_2210057
Anti-Tubulin	Tab-IP (Curie Institute)	A-R-H#02
Anti-gamma Tubulin	Sigma	T6557; RRID: AB_477584
Anti-pericentrin	Abcam	ab4448; RRID: AB_304461
Anti-pericentrin	BD Biosciences	611815; RRID: AB_399295
Anti-polyglutamylated Tubulin	Tab-IP (Curie Institute)	A-R-H#04
Anti-Vimentin	Cell Signaling	5741S; RRID: AB_10695459
Anti-p150 glued	BD Biosciences	612709; RRID: AB_399948
Chemicals, Peptides, and Recombinant Proteins		
Nocodazole	Sigma	M1404
Y27632	Sigma	Y0503
Paraformaldehyde	Euromedex	15710
Glutaraldehyde	Sigma	G5882
Phalloidin-A555	Life Technologies	A34055
Phalloidin-A568	Life Technologies	A12380
DAPI	Sigma	D9542
PLL(20)-g[3.5]-PEG(2)	SurfaceSolutionS	PLL(20)-g[3.5]-PEG(2)
PLPP (4-benzoylbenzyl-trimethylammonium chloride)	Alveole	PLPP
Ti-Prime	MicroChemicals	Ti-Prime
Polystyrene MW 260,000	Acros Organic	178891000
Toluene	Sigma	179418
Fibronectin	Sigma	F1141
Experimental Models: Cell Lines		
MEF WT and KO Vimentin cells	John Eriksson, Robert Goldman	Cheng et al.[51] and Mendez et al.[52]
Recombinant DNA		
p150-CC1 (214-548 aa of p150Glued)	Mineko Kengaku	Wu et al.[60]
Software and Algorithms		
ImageJ 1.52o	http://imageJ.nih.gov/ij	Colucci-Guyon et al.[65]
μManager	micro-manager.org	Stuurman et al.[66]
Java 1.8.0	Oracle Corporation	https://www.java.com/fr/download/
R 4.0.2 GIU 1.72 Catalina build (7847)	R Core Team	https://www.r-project.org/
Rstudio 1.2.1335	R Studio, PBC	https://rstudio.com/
Prism 9 for macOS	GraphPad Software	https://www.graphpad.com/scientific-software/prism/
Metamorph	Molecular Devices	https://www.moleculardevices.com/products/cellular-imaging-systems/acquisition-and-analysis-software/metamorph-microscopy
μManager-Leonardo plugin	Alveole	Leonardo
CleWin layout editor software	WieWeb	CleWin

(*Continued on next page*)

Please cite this article in press as: Jimenez et al., Acto-myosin network geometry defines centrosome position, Current Biology (2021), https://doi.org/10.1016/j.cub.2021.01.002

Continued

REAGENT or RESOURCE	SOURCE	IDENTIFIER
Other		
SCHOTT NEXTERION Coverslips #1.5H "High Performance	SCHOTT	SCHOTT NEXTERION Coverslips #1.5H "High Performance
Photomask	Toppan Photomask	Quartz grade D (MFS > 1μm).
NEPA21 electroporator	Nepa Gene	NEPA21
Plotter-cutter	GRAPHTEC	CE-6000-40
Air-plasma	Plasma Etch	PE-30
Primo module	Alveole	Primo
Spin-coater	Laurell	WS-650m2-23NPPB
UVO cleaner	Jelight	Model No. 342A-220
Nikon microscope Ti-E equipped with a CFI Super Plan Fluor 20 × ELWD (NA 0.45) objective capable of high UV-transmission, a Perfect Focus System 3, an ORCA-Flash 4.0 LT CMOS camera (Hamamatsu), a motorized stage (Märzhäuser)	Nikon, Hamamatsu, Märzhäuser	Gattaca for custom configuration of microscope set-up
Olympus up-right BX61 equipped with a CoolSnapHQ2 (Photometrics) camera with a motorized stage (Märzhäuser)	Olympus, Photometrics, Märzhäuser	Gattaca for custom configuration of microscope set-up
Inverted spinning disk microscope Nikon Ti2 equipped with a Retiga R3 camera (Photometrics), a motorized stage (Märzhäuser)	Nikon, Photometrics, Märzhäuser	Gattaca for custom configuration of microscope set-up

RESOURCE AVAILABILITY

Lead contact

Further information and requests for resources and reagents should be directed to and will be fulfilled by the Lead Contact, Manuel Théry (manuel.thery@cea.fr).

Materials Availability

All materials generated for this study are available upon request.

Data and Code Availability

The datasets supporting the current study have not been deposited in a public repository because they are too large (more than 10To) but are available from the corresponding or the first author on request.

The code supporting the current study has not been deposited in a public repository because it has not been formated to be user friendly and has not been annotated therefore it requires further detailed explanation to be used but is available from the corresponding or the first author on request.

EXPERIMENTAL MODEL AND SUBJECT DETAILS

Cell lines

MEF (mouse embryonic fibroblasts) WT and KO Vimentin cells: Vimentin heterozygous mice (129/Sv × C57BL/6) were used to generate vimentin-deficient homozygotes and WT mice and MEF cells by the lab of John Eriksson.[50–52] The information of the sexe or the developmental stage from which the cells were extracted is not available.

RPE1 (Retinal pigment pithelium) puromycin sensitive cells were obtained from Andrew Holland and were not further characterized.

PTK2 (Potorous tridactylus kidney) cells were obtained from Franck Perez lab and were not further characterized.

C2C12 (Mouse muscle myoblast) cells were obtained from Jean-Louis Viovy lab and were not further characterized.

Cell Culture

Cell culture, cell lines, plasmids and transfection and drug treatment.

MEF WT and KO for Vimentin cell lines (received from Robert Goldman), C2C12 and PTK2 cells were cultured in Dulbecco's Modified Eagle Medium (31966, GIBCO) supplemented with 10% FBS (50900, Biowest) and 1% antibiotic-antimycotic (15240-062, GIBCO). RPE1 cells were cultured in Dulbecco's Modified Eagle Medium Nutrient Mixture F-12 (31331-093, GIBCO) supplemented

Please cite this article in press as: Jimenez et al., Acto-myosin network geometry defines centrosome position, Current Biology (2021), https://doi.org/10.1016/j.cub.2021.01.002

with 10% FBS and 1% antibiotic-antimycotic. All cells were grown in 37°C, 5% CO2 conditions. MEF KO Vimentin EGFP-Centrin 1 were made by transient transfection of pEGFP-C1-Centrin1 (kindly provided by James Sillibourne) with lipofectamine LTX (15338100, Invitrogen) in Opti-MEM (11058, GIBCO) according to the procedure described by the manufacturer. Selection was performed with G418 at 0.5mg/mL and sorted by FACS twice with one month interval. They were posteriorly cultured with 0.2mg/mL. For p150 inhibition assay on cytoplasts, we used WT MEF instead of vimentin KO MEF to avoid confusion between GFP from centrin1 and from the p150 construct, or RPE1 cells. Centrosome positioning was similar in both cells lines (Figures S7C and S7D). Cells were electroporated with NEPA21 electroporator (from Nepa Gene) with the plasmid expressing GFP-p150-CC1 (214-548 aa of p150Glued) obtained from Mineko Kengaku (Kyoto University) and according to the manufacturer's protocole for MEF cells. Cells were then sorted by FACS 24 h after electroporation and plated directly on slides for enucleation and enucleated 48 h after electroporation. Living cells were incubated and imaged at 37°C with 5% CO2 in a humidified environment.

METHOD DETAILS

Enucleation

Cells were seeded the night before, 12 h before enucleation on RINZL plastic micro-slides (71890-01, Delta Microscopies) precoated with Collagen I Rat Protein, Tail (A1048301, GIBCO) at 12μg/mL and Fibronectin from bovine plasma (F1141, Sigma) at 1μg/mL for 1 h. Cells were seeded to achieve a 90% confluence by the time of the enucleation. Cells were put on 50ml tubes resistant to high-speed centrifugation (339652, Nunc) in complete medium with Cytochalasin D (C8273, Sigma) at 3μg/mL for 30min at 37°C, then centrifuged at 15'000 g for 1 h at 37°C. Cytoplasts were then washed twice with pre-warmed DMEM then let them to rest for 30min at 37°C before detachment for seeding on micropatterns. An alternative protocole was used for C2C12 cells. In this case, cells were seeded the night before on RINZL slides pre-coated with Fibronectin (at 10μg/mL for 40min). On the day of the experiment, cells were incubated with Cytochalasin D at 2μg/mL for 45min at 37°C, then centrifuged at 10'000rpm at 37°C using an ultra-centrifuge (Avanti JXN-26, Beckman Coulter) equipped with a swinging rotor (JS-13.1, Beckman Coulter).

Drug treatment

Microtubules were removed by incubating cells in HBSS (14025092, GIBCO) on ice and in a cold room at 4°C for 2 h then warmed up to 37°C in complete medium with 10μM Nocodazole (M1404, Sigma) and incubated until fixation. Rock inhibition was achieved with Y27632 (Y0503, Sigma) at 20μM. Rock inhibition in the absence of microtubules was achieved with cold incubation as described above and warming up with complete medium with 10μM Nocodazole and Y27632 at 100 or 200μM as specified for 2 h at least.

Fixation and Immunostaining

Cells plated on coverslips were fixed with Paraformaldehyde (15710, Euromedex), Glutaraldehyde (G5882, Sigma) or a mixture of both depending on the antibodies used. All fixation mixtures were done in Cytoskeleton Buffer supplemented with Sucrose (CBS, see below) with 0.1% Triton X-100 (T8787, Sigma) with either 3% Paraformaldehyde, 3% Paraformaldehyde + 0.025% Glutaraldehyde or 0.5% Glutaraldehyde. Fixation mixture was added to the cells for 10 min at room temperature. Glutaraldehyde related autofluorescence was quenched with a solution of PBS and 1mg/mL sodium Borohydride for 10 min at room temperature. Cells were then re-permeabilized with Triton 0.1% in PBS for 10 min at room temperature, then blocked with Bovine Serum Albumin (BSA, A2153, Sigma) at 1.5% in PBS for 10 min. Antibodies were diluted in PBS containing 1.5% BSA and both incubation with primary or secondary antibodies was made for 1 h. Microtubules were stained with MCA77G from Abd serotec, ab18251 from Abcam or A-R-H#02 from Tab-IP (Curie Institute antibody platform). Centrosome staining was performed with anti-gamma Tubulin (T6557,Sigma), anti-pericentrin (ab4448, Abcam-for human and Ptk2 cells; 611815, BD Biosciences-for mice cells) or anti-polyglutamylated Tubulin (A-R-H#04, TabIP platform, Institut Curie). Vimentin was stained with 5741S from Cell Signaling using methanol fixation for 5min at −20°C . Dynein was stained with anti-p150 glued antibodies (612709, BD Biosciences). A particular protocole was used for Dynein staining with an extra step of pre-permeabilization using 0.025% Triton X-100 in CBS for 30 s followed by fixation in 4% PFA + 0.05% Glutaraldehyde + 0.1% Triton X-100 in CBS for 10 min. Actin filaments were stained with Phalloidin-A555 (A34055, Life Technologies) or Phalloidin-A568 (A12380, Life Technologies) together with secondary antibodies. Staining with DAPI (D9542, Sigma) was performed systematically with secondary antibodies to stain the nucleus or to control proper enucleation. Coverslips were mounted with Mowiol 4-88 (81381, Sigma).

Cytoskeleton Buffer supplemented with Sucrose (CBS): A stock solution containing 10 mM HEPES (H3375, Sigma) at pH 6.1, 138 mM KCl (P3911, Sigma), 3 mM MgCl2 (208337, Sigma) and 2 mM EGTA (E3889, Sigma) was made. Sucrose was added extemporaneously before use at 0.32M (10%).

Micropatterning

Micropattern prototyping using Primo

The micropatterning protocol was adapted from.[67]

Micropattern were obtained by shining a pattern of UV light through the microscope objective on a PEGylated glass coverslip covered with a liquid containing a photo-initiator. To limit the volume of liquid to use for the process (here choose at 30 μl), a custom silicone chambers was assembled using two sandwiched 250μm silicon sheets, cut with a plotter-cutter (GRAPHTEC CE-6000-40). For the bottom layer a millimeter pear shape in-between inlet and outlet channels (0.5 um wide), and for the top layer, holes upward

Please cite this article in press as: Jimenez et al., Acto-myosin network geometry defines centrosome position, Current Biology (2021), https://doi.org/10.1016/j.cub.2021.01.002

the end of the inlet and outlet channels. 18x18 SCHOTT NEXTERION Coverslips #1.5H "High Performance" were used for prototyping steps. Coverslips were handles under a laminar flux hood. To promote attachment of PDMS chambers then attachment of Poly-l-Lysine-Polyethylenglycol/PLL-PEG, the surface of the coverslips was oxidized 40 s by exposure to air-plasma (PE-30, Plasma Etch) at 30W, under vacuum and with an air flow rate of 10 cc/minute. Then the silicone chamber was put onto the activated side followed by the introduction of PLL-PEG solution from the inlet channel. The PLL-PEG solution (PLL(20)-g[3.5]-PEG(2), SurfaceSolutionS, Switzerland), at a concentration of PLL-PEG at 0.1mg/mL in 10mM HEPES at pH7.4, was incubated for 30 min at room temperature. This step was performed extemporaneously, right before patterning. The coverslip was avoided to dry after this step and during and between all following steps. The coverslip was washed once with of PLPP (4-benzoylbenzyl-trimethylammonium chloride, 14.5cmgcml−1) then fresh PLPP was added, by removing most of the liquid at the outlet with a highly absorbant precision paper (Kimwipes, Kimtech). Surface patterning was performed right after on an inverted Nikon microscope Ti-E equipped with a CFI Super Plan Fluor 20 × ELWD (NA 0.45) objective capable of high UV-transmission, a Perfect Focus System 3, an ORCA-Flash 4.0 LT CMOS camera (Hamamatsu), a motorized stage (Märzhäuser) and the Primo module containing a DMD illumination with a 375cnm (4.5cmW) laser (Alvéole Lab). The microscope was controlled with the ImageJ μmanager software and the Primo module was controlled with the μManager-Leonardo plugin (Alvéole Lab). Micropattern shapes were designed using ImageJ, as an 8bit image with patterns filled in white on a black background. Each field was exposed for 25 s at 100% UV power corresponding to a 900 mJ/mm2 UV energy dose. The coverslips were washed 3 times with PBS by pipetting 100ul in the inlet while aspirating at the outlet using a high absorbant precision paper to create a flow within the chamber. Coverslips were then incubated with Fibronectin at 20μg/mL in PBS for 20 min by flowing 100μl of the solution, and then washed 3 times with PBS as described above. The silicone chamber assembly can be detached at this step by immersing coverslips in PBS and using tweezers. Patterned sample were kept at 4°C in PBS and used the next day. Cells were plated as described bellow for deep UV patterning.

Large scale micropatterning with deep UV and cell seeding

The micropatterning protocol was adapted from.[68]

Polystyrene coating: 20x20 Coverslips (1304369, Schott) were cleaned for 10min in acetone then for 10min in isopropanol in a bath sonicator and then dried with compressed-clean air under a laminar flow hood. They were coated with adhesion promoter Ti-Prime (MicroChemicals) using a spin-coater (WS-650m2-23NPPB, Laurell) at 3000 rpm for 30 s and baked on top heater for 2min at 120°C. Then a 1% polystyrene (MW 260,000, 178891000, Acros Organic) solution in toluene (179418, Sigma) was spin-coated on the coverslip at 1000 rpm.

Plasma treatment and micropatterning: Polystyrene layer was oxidized by exposure to air-plasma as described above to promote the attachment of PLL-PEG to the surface, which was diluted as described above and incubated for 30min at room temperature. PLL-PEG was removed and coverslips room air-dried before putting them in tight contact with a chromed printed photomask (Toppan Photomask). Tight contact was maintained using a vacuum holder. The PLL-PEG layer was burned with deep UV (λ = 190nm) through the non-chromed windows of the photomask, using UVO cleaner (Model No. 342A-220, Jelight), at a distance of 1cm from the UV lamp with a power of 6mW/cm2, for 4 min.

Cell seeding: Coverslips were washed once with distilled water then incubated with a solution of 40μg/mL Fibronectin (F1141, Sigma) in PBS (14190169, GIBCO) for 30min at room temperature. Coverslips were then washed, in a sterile 6-well dish with one coverslip per well and under the laminar flow hood, 3 times with 3ml sterile PBS, once with 3ml DMEM and once with 3ml DMEM-10%FBS-1%Antibiotic-Antimycotic (complete medium). Cells/cytoplasts were detached with TrypLE (12605036, GIBCO), centrifuged and resuspended in complete medium at 100'000 cells/mL. Most medium was removed for each well containing a coverslip and 1ml of cell suspension was added. Cells were left for spreading for 1 h at 37°C before washing-out non-attached cells with pre-warmed complete medium. Cells were incubated for at least one more h at 37°C to promote correct spreading and polarization, before further treatments.

Imaging

Microscopy

Most fixed and fluorescently labeled cells were imaged using an up-right epi-fluorescence microscope (Olympus up-right BX61 equipped with a CoolSnapHQ2 camera) monitored by Metamorph. Samples were scanned for cell selection with dry objectives 10x or 20x using a Metamorph plugin developped by Céline Labouesse and Benoît Vianay. Cells were chosen so that they were well spread on sharp patterns and that they do not had a nucleus in the case of conditions with cytoplasts. Cells were imaged with a 100x NA 1.4 oil objective, with 0.5μm spacement between z planes in a range of 15μm. When patterned cells did not fit in one camera field, overlapping images were taken for further stitching. An inverted spinning disk microscope (Nikon Ti2 equipped with a Retiga R3 camera), monitored by Metamorph was used for Figure 7C and Figure S1D using a 60X objective.

Image analysis

For patterned cells that could not fit in one camera field, ImageJ[69] macros using Stitching plugin were used. Images were then processed the same than single images.

Centrosome positioning analysis was performed with homemade ImageJ suite of macros. The closest plane to the coverslip (cell bottom) was determined creating a band ROI on the actin image, as an expansion of a rough cell border determined by threshold filtering. This ROI was applied to the microtubule channel where the z-plane with the highest Standard Deviation within the band was chosen as cell bottom. Cell Top was determined using the standard deviation of the whole image. Firsts and lasts superfluous z-planes were that way removed to lighten calculations.

Please cite this article in press as: Jimenez et al., Acto-myosin network geometry defines centrosome position, Current Biology (2021), https://doi.org/10.1016/j.cub.2021.01.002

Threshold filtering in actin cell bottom plane was performed to determine cell edges and centroid was calculated. Similar method was used to determine nucleus edges and centroid in the case of conditions with nucleated cells. Scanning the Prominence parameter of the "Find Maxima" plugin from imageJ was performed to determine the prominence value where the number of found maxima was closest to one. Scanning for maxima within the region around this principal centriole was performed to find eventual extra-centrioles. Cells with more than 4 centrioles were discarded. The centroid of the polygon defined after connecting all centrioles 3 by 3 into triangles and adding all areas was used for the calculation of the distances to the cell, and nucleus if applicable, centroids.

All steps contained a quick-scanning verification and assisted-correction module to make sure the analysis was correct for all cells.

Centrosome positioning compared triangle characteristic centers

In the case of triangle-patterned cytoplasts, the contour defined previously was smoothened by converting curve into a spline defined by a discrete number of close points. The curve defined by the distance of each point from the spline to the previously calculated centroid was smoothened by quadratic regression until the curve presents only 3 maxima, corresponding to the 3 triangle vertexes. The indexes of these three points were used to find the 3 corresponding points the contour-spline. The coordinates of theses 3 points were used to fit the contour of the cell to a triangle. Geometrical calculations were performed to determine the coordinates of 4 characteristic centers of that triangle (centroid, incenter, circumcenter, and orthocenter). Distances from the centrosome to these centers were calculated.

Actin inner zone (AIZ) and actin inner center (AIC)

Actin inner zone was determined manually on projected and denoised (rolling ball filtering) actin images. The coordinates centroid of the zone was determined and the distance to cell and centrosome centroids was calculated.

Dot plots and plots of AIZs

An angle correction was determined for all cells in a semi-automatic way. The coordinates of all centers were redressed according to the correction angle and relative coordinates to cell or actin centroid were calculated and plotted. Similar procedure was performed for the regions defining AIZs. Either all contours of AIZs were drawn, or one black 8-bit image was created for each cell and the AIZs was drawn and filled in white. A sum of all the images was made and a Royal LUT was applied.

Microtubule orientations

Microtubule stacks were skeletonized using a homemade Java plugin. A sum projection was made before a homemade orientation filter was applied to determine the angle made by each pixel of the skeletonized microtubule network. The calculation of a relative angle to the centrosome was performed. This angle corresponds to the angle made locally by a portion of microtubule around a given pixel and the radius defined by the line passing by both the studied pixel and the centrosome. The distribution of relative angle value as a function of the distance to the centrosome was determined and plotted with R. This distribution was also performed this time limiting the considered values to a band as shown in the figures or to a given zone like the AIZ.

QUANTIFICATION AND STATISTICAL ANALYSIS

Mann-Whitney non-parametric tests were used in the entire study to compare samples using GraphPad Prism software (Version 6.0). Statistical details of experiments can be found in the figure legends, including exact value of n, which represent the number of cells. The center of distributions correspond to the medians, except in Figure 3B where it correspond to the average. The measures of the width of the distributions are standard deviations, except in Figure 3B where it is the standard error mean (SEM).